

APPLIED RESEARCH

Bayesian Inference for Thermal Model of Synchronous Generator—Part I: Parameter Estimation

MADHUSUDHAN PANDEY AND BERNT LIE , (Member, IEEE)

Telemark Modeling and Control Center (TMCC), 3901 Porsgrunn, Norway

Corresponding author: Bernt Lie (bernt.lie@usn.no)


ABSTRACT Due to the increasing injection of intermittent power sources (solar+wind) into a common grid, dispatchable sources such as hydro power should be able to help reduce the variability in load and the variability in generation caused by the intermittent sources. A hydro generator should be able to operate short-term beyond its thermal capability limit. This requires the monitoring of internal temperatures in the hydro generator. In this paper, a thermal model of an air-cooled synchronous generator is presented, emphasizing the various aspects of parameter estimation and identifiability using Bayesian inference. Inferences are drawn from the posterior distributions of the parameters and initial conditions, dispersion (spreading) of particles and sampling efficiency, practical parameter identifiability, and model mismatch with experiments. Results show extremely narrow parameter distributions. It is early to generalize about the posterior distribution of air-related and metal-related parameters of the air-cooled synchronous generator based on the single experimental data presented here.

INDEX TERMS Bayesian inference, model fitting, parameter estimation, parameter identifiability, synchronous generator, thermal model.

I. INTRODUCTION

Electricity generation from intermittent sources such as solar power, wind power, tidal power, etc., is rapidly increasing in modern electric power system networks. The intermittency in these sources causes the power system networks to operate in different operating conditions. Dispatchable sources such as hydro power can be used for removing the variability in the system's power production caused by the intermittent sources [1], [2], [3], [4]. Thus, in a modern power system, the hydro generators play a significant role in the flexible operation of the intermittent grid. A concept of flexible hydro power is coined in [5] for modern intermittent power system networks. This adheres to a new research requirement in the case of a synchronous hydro generator operating in tandem with the intermittent sources. The performance of the synchronous generator depends on its capability diagram [6]. The capability diagram provides information about the oper-

ating regimes of the synchronous generator in case of the various operational limits, viz., armature current limit, field current limit, and under-excitation [7]. In [6], an instance of exploiting more active power from the hydro generator is studied by controlling the internal temperature of the machine. The control of the armature current limit and the field current limit will result in a decrease in resistance of the armature and the field winding due to temperature monitoring of the rotor copper, stator copper, and stator iron. Furthermore, because of an increase in the active current through the synchronous generator, more active power can be exploited. The temperature is controlled by cooled air circulation through the generator's internal surfaces. The cooled air is supplied through a heat exchanger, in a closed loop. Previous work includes a brief review of thermal analysis of electrical machines [8]. Lumped-parameter thermal network (LPTN) models of the thermal machines are provided in [9], [10], and [11]. Finite element analysis (FEM), and computational fluid dynamics (CFD) models were studied in [12] and [13]. A totally enclosed water-cooled thermal model

The associate editor coordinating the review of this manuscript and approving it for publication was Bo Shen .

of synchronous machines for an electric vehicle has been proposed in [14]. More recently, a totally enclosed thermal model of an air-cooled hydro generator has been developed in [15] using a closed-loop heat exchanger model for cooling heated air from the outlet of the generator. The thermal model of the air-cooled generator is further extended in [16] with the inclusion of temperature-dependent electrical resistances, temperature-dependent specific heat capacities of the metals, and fluids (air+water) inside the air-cooled hydro generator. The model of the air-cooled hydro generator is represented by a computationally cheap online solution of the non-linear model of the heat exchanger in [17], where a hybrid model (mechanistic+data-driven) is proposed using linear and non-linear regression.

In Section II, materials and methods are outlined. Section III provides the mathematical governing equations for the air-cooled hydro generator. In Section IV, results from parameter estimation and parameter identifiability using Bayesian inference are discussed. Conclusions are drawn in Section V with future work suggested in Section VI.

II. MATERIALS AND METHODS

A. SYSTEM DESCRIPTION

Figure 1 shows the working principle of a thermal model of an air-cooled synchronous hydro generator. The cold air out of the heat exchanger is blown by a fan into the rotor/stator air gap. The air is heated by heat flow from the rotor, air gap windage, and bearing friction. Furthermore, the air is forced into the iron cores and then gets heated by the heat flow from the iron cores. The heated air is now collected at the stator's outlet and passed through a counter current heat exchanger. The heated air is cooled using continuous cold water circulation in the heat exchanger and then fed again into the air gap as a closed loop process. The heat exchanger is provided with cold water, with mass flow rate \dot{m}_w , at temperature T_w^c . The air mass flow rate is \dot{m}_a with temperature T_a^h at stator outlet and heat exchanger entry. The rotor copper heat source, \dot{Q}_r^σ , is due to eddy currents caused by I_f . Similarly, the stator copper heat source, \dot{Q}_s^σ , is due to stator terminal current I_t . \dot{Q}_{Fe}^σ is stator iron heat source, and \dot{Q}_f^σ is heat generated due to friction in the stator/rotor air gap. The thermal operation of the air-cooled synchronous generator is mainly influenced by \dot{m}_w , \dot{m}_a , T_w^c , \dot{Q}_{Fe}^σ , \dot{Q}_f^σ , I_t , and I_f . It is of interest to consider evolution of temperature in the rotor, stator, and iron core indicated by T_r , T_s and T_{Fe} , respectively. Monitoring of these temperatures allows for optimal exploitation of active power production by enhancing the capability diagram to a new regime of operation [6].

Figure 2 shows the Bayesian framework for inference about parameters of a dynamical system. In the figure, x, u, z, θ , and y are the states, inputs, algebraic variables, parameters, and outputs, respectively. In the figure, $p(\theta)$ is the prior probability distribution of θ , $p(y | \theta)$ is the likelihood function, and $p(\theta | y)$ is the estimated posterior distribution of θ . Section IV provides detailed explanation about

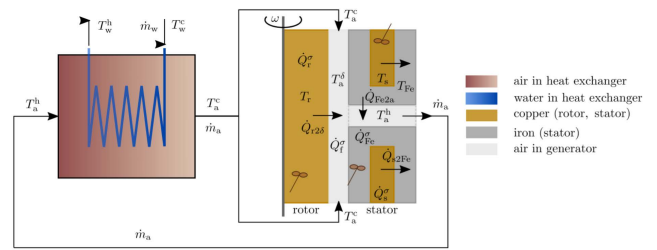


FIGURE 1. Thermal model of the synchronous generator taken from [16].

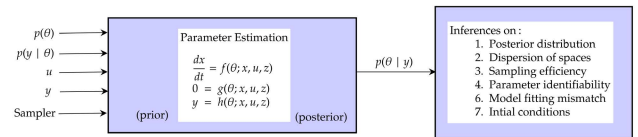


FIGURE 2. Bayesian inference for the parameter estimation.

priors and likelihood. In Fig. 2, we also see that the posterior distribution of parameters allows for various inferences about the parameters of a dynamical system. The inferences include (i) finding statistical moments from the posterior distribution of the parameters, (ii) finding the relative dispersion of the parameter space and the relative sampling efficiency between the parameters, (iii) model mismatch with experiment and (iv) inferences related to the posterior distribution of the initial conditions while working with the model and the experimental data offline.

B. EXPERIMENTAL DATA

A heat-run test, of the synchronous machine, was performed for 600 min [15] with sampling rate = [1] min. Only data from $t = 16$ min to $t = 600$ min, i.e., 584 data points, will be used for model fit. For each minute, for a supplied field current, starting from a cold-start, measurements for different quantities are recorded. The cold-run last up to 53 min, where the terminal voltage is built-up due to residual flux in rotor windings. The measurements are available for both electrical quantities and temperatures related to the air-cooled synchronous generator. After the cold-run, the field current is increased which increases the temperature of the stator copper and the stator iron. The measured quantities are summarized in Table 1, and the experimental data are plotted in Fig. 3. The expression for terminal current I_t as shown in Table 1, indicates that it is not measured using a sensor, however calculated from a mathematical expression relating power and voltage.

III. MATHEMATICAL MODEL

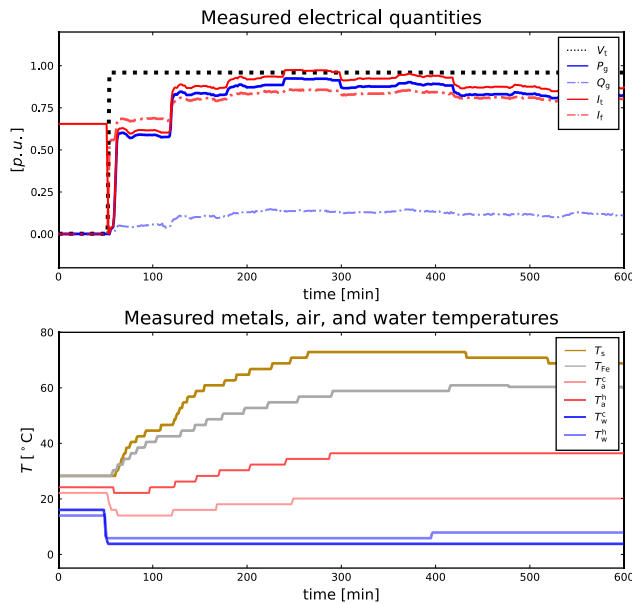
The mathematical equations governing generator metal temperatures taken from [16] and [18] are

$$m_r \hat{c}_{p,Cu} \frac{dT_r}{dt} = 1.1 R_r I_f^2 - U A_{r2s} (T_r - T_a^\delta) \quad (1)$$

$$m_s \hat{c}_{p,Cu} \frac{dT_s}{dt} = 3 R_s I_t^2 - U A_{s2Fe} (T_s - T_{Fe}) \quad (2)$$

TABLE 1. Measured quantities from a 600 min heat-run test.

Quantity	Symbol	Units	Sensor
Generator terminal voltage	V_t	kV	-
Active power of generator	P_g	MW	-
Reactive power of generator	Q_g	MVar.	-
Rotor field current	I_f	A	-
Temperature of stator	T_s	$^{\circ}\text{C}$	PT 100
copper			
Temperature of stator iron	T_{Fe}	$^{\circ}\text{C}$	PT 100
Hot air temperature	T_a^h	$^{\circ}\text{C}$	Pt 100/CTD
Cold air temperature	T_a^c	$^{\circ}\text{C}$	Pt 100/CTD
Cold water temperature	T_w^c	$^{\circ}\text{C}$	Analog
Hot water temperature	T_w^h	$^{\circ}\text{C}$	Analog
Terminal current	$I_t = \frac{P_g^2 + Q_g^2}{\sqrt{3}V_t}$	A	-


FIGURE 3. Experimental data for generator model from a 600 min heat-run test taken from [15].

$$m_{\text{Fe}} \hat{c}_{p,\text{Fe}} \frac{dT_{\text{Fe}}}{dt} = \mathcal{U}A_{s2\text{Fe}}(T_s - T_{\text{Fe}}) - \mathcal{U}A_{\text{Fe}2a}(T_{\text{Fe}} - T_a^h) + \dot{Q}_{\text{Fe}}^{\sigma}. \quad (3)$$

Similarly, the dynamical equations for air inside the generator are

$$0 = \dot{m}_a \hat{c}_{p,a}(T_a^c - T_a^{\delta}) + \mathcal{U}A_{r2\delta}(T_r - T_a^{\delta}) + \dot{Q}_f^{\sigma} \quad (4)$$

$$0 = \dot{m}_a \hat{c}_{p,a}(T_a^{\delta} - T_a^h) + \mathcal{U}A_{\text{Fe}2a}(T_{\text{Fe}} - T_a^h), \quad (5)$$

and the heat exchanger is model as

$$(N_{\text{St}}^w - N_{\text{St}}^a e^{-N_{\text{St}}^{\Delta}})T_a^c = N_{\text{St}}^{\Delta}T_a^h + N_{\text{St}}^a(1 - e^{-N_{\text{St}}^{\Delta}})T_w^c. \quad (6)$$

In Eq. 6 N_{St}^i for $i \in \{w, a, \Delta\}$ are dimensionless Stanton numbers relating heat transfer coefficient, density, heat capacity, and velocity.

Equations 1-6 can be written in Differential Algebraic Equations (DAEs) form as

$$\frac{dx}{dt} = f(x, z, u; \theta)$$

$$0 = g(x, z, u; \theta)$$

$$y = h(x, z, u; \theta) \quad (7)$$

where $x = (T_r, T_s, T_{\text{Fe}})$, $z = (T_a^c, T_a^{\delta}, T_a^h)$, $u = (I_f, I_t, T_w^c)$,

$$\theta = (m_r, m_s, m_{\text{Fe}}, R_r, R_s, \hat{c}_{p,\text{Cu}}, \hat{c}_{p,\text{Fe}}, \hat{c}_{p,a}, \dot{m}_a, \mathcal{U}A_{r2\delta}, \mathcal{U}A_{s2\text{Fe}}, \mathcal{U}A_{\text{Fe}2a}, \dot{Q}_{\text{Fe}}^{\sigma}, \dot{Q}_f^{\sigma}, N_{\text{St}}^a, N_{\text{St}}^w, N_{\text{St}}^{\Delta}).$$

The parameters and operating conditions are given in Table 2.

Out of the three states, T_s and T_{Fe} are measured, while it is of interest to estimate the temperature of rotating rotor copper T_r . Similarly, out of three algebraic variables, T_a^c and T_a^h are measured, and it is also of interest to estimate air gap temperature T_a^{δ} . The measured inputs, states and algebraic variables are shown in Fig. 3.

IV. PARAMETER ESTIMATION

A. PROBLEM FORMULATION

It is of interest to estimate the thermal parameters and initial conditions of the air-cooled hydro generator using Bayesian inference.

The expected value of parameter $\hat{\theta}$ is calculated as

$$\hat{\theta} = \arg \max_{\theta} p(\theta | y),$$

where $p(\theta | y)$ is the ‘‘posterior probability distribution of parameter θ for the given data y ’’. $p(\theta | y)$ is expressed in terms of likelihood $p(y | \theta)$ and prior $p(\theta)$,

$$p(\theta | y) = \frac{p(y | \theta)p(\theta)}{p(y)} \quad (8)$$

where $p(y)$ is independent of θ , and is used as a normalization constant for $p(\theta | y)$. $p(y)$ is also known as the evidence or the marginal likelihood. The prior $p(\theta)$ is our prior beliefs about the probability density function for the parameter θ without seeing the data. Similarly, the likelihood $p(y | \theta)$ is a model representing the distribution of the data given a fixed parameter θ and calculated as

$$p(y | \theta) = \prod_{i=1}^N p(y_i | \theta).$$

The evidence $p(y)$ used for normalization is calculated as the joint probability distribution of $p(\theta | y)$ and $p(y)$

$$p(y) = \int p(\theta | y)p(y) d\theta. \quad (9)$$

The analytical solution to Eq. (9) is only available for simple cases, and in real-life Bayesian inference, numerical solutions are used. The Bayesian parameter estimation method is applied to the system given by Eqs. (1-6).

B. FORMULATION USING TURING.JL

Turing.jl is a Julia package for probabilistic programming [19]. Turing.jl is also composable with DifferentialEquations.jl [20], a Julia package for differential equations, facilitating Bayesian inference in the parameter of the system

TABLE 2. Parameters and initial operating conditions.

Quantities	Symbols	Values
Mass of rotor copper, stator copper and stator iron	m_r, m_s, m_{Fe}	9260 kg, 6827 kg, 71200 kg
Ohmic resistances of rotor copper and stator copper	R_r, R_s	0.127 Ω , 1.95 m Ω
Specific heat capacities of copper and iron	$\hat{c}_{p,Cu}, \hat{c}_{p,Fe}$	0.385 kJ/kg/K, 0.465 kJ/kg/K
Specific heat capacities of air and water	$\hat{c}_{p,a}, \hat{c}_{p,w}$	1.15 kJ/kg/K, 4.2 kJ/kg/K
Air and water mass flow rates	\dot{m}_a, \dot{m}_w	49.2 kg/s, 53.9 kg/s
Heat transfer, rotor to air gap, stator copper to iron, and stator iron to air	$\mathcal{U}A_{r2\delta}, \mathcal{U}A_{s2Fe}, \mathcal{U}A_{Fe2a}$	2.7 kW/K, 20 kW/K, 14.3 kW/K
Stator iron generated heat	\dot{Q}_{Fe}^σ	212 kW
Friction heating	$\dot{Q}_f^\sigma = 0.8 \cdot \dot{W}_f$	422.4 kW
Friction work	\dot{W}_f	528 kW
Stanton number, air	$N_{St}^a = \frac{\mathcal{U}A_x}{\hat{c}_{p,a}\dot{m}_a}$	0.785
Stanton number, water	$N_{St}^w = \frac{\mathcal{U}A_x}{\hat{c}_{p,w}\dot{m}_w}$	0.196
Stanton number, difference	$N_{St}^\Delta = N_{St}^w - N_{St}^a$	-0.589
Heat transfer, air to water	$\mathcal{U}A_x = 1 / \left(\frac{1}{h_a A_x} + \frac{1}{h_w A_x} \right)$	44.46 kW/K
Heat transfer, solid to air	$h_a A_x$	55.6 kW/K
Heat transfer, solid to water	$h_w A_x$	222 kW/K
Initial value of rotor copper, stator copper, and stator iron temperatures	$T_a^c(t=0), T_s(t=0), T_{Fe}(t=0)$	28°C, 28°C, 28°C
Initial value of cooled air, air-gap, and hot air temperatures, stator copper, and stator iron temperatures	$T_a^c(t=0), T_a^\delta(t=0), T_a^h(t=0)$	14°C, 18°C, 22°C

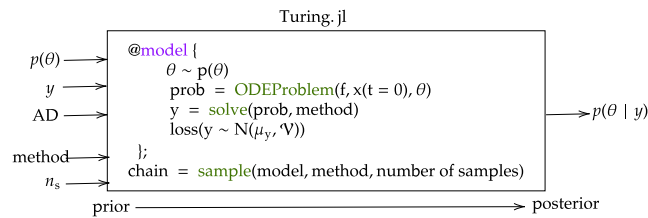


FIGURE 4. Bayesian inference implemented in Turing.jl in the Julia language.

represented by differential equations. The problem is formulated as shown in Fig. 4.

For the differential equations represented by Eqs. (1-6) we want to estimate posterior distributions of:

- initial states $T_r(t=0), T_s(t=0)$, and $T_{Fe}(t=0)$
- heat transfer coefficients $\mathcal{U}A_{r2\delta}, \mathcal{U}A_{s2Fe}, \mathcal{U}A_{Fe2a}$, and $\mathcal{U}A_x$
- heat sources \dot{Q}_{Fe}^σ and \dot{Q}_f^σ .

Table 3 shows the priors and the data for the estimation of the selected parameters. In the table, \mathcal{V} , usually chosen as an inverse gamma function mostly for measurement sequence in Bayesian inference [21], is the prior to the variance of the measurement noise where we assume $\mathcal{V} \sim \Gamma^{-1}(2, 3)$. We have assumed that all measurements have the same noise variance since all temperatures are of similar size. The measurement vector is $y = (T_s \ T_{Fe} \ T_a^c \ T_a^h)$. A loss function is formulated using Turing.jl. The priors for the initial rotor copper temperature are truncated normal distributions. For parameters θ such as initial descriptor (differential and algebraic variables) as well as model constants, it is common to

assume a normal distribution, e.g., $\theta \sim \mathcal{N}(\mu, \sigma)$. Because we normally want to limit the distribution to lie within a range $\theta \in [\theta_{min}, \theta_{max}]$, e.g., to avoid negative values, it is quite common to use a truncated normal distribution for the prior of θ ,

$$\theta \sim \mathcal{T}(\mathcal{N}(\mu, \sigma), \theta_{min}, \theta_{max})$$

where \mathcal{T} represents truncated normal distribution for θ . The prior to the initial rotor copper temperature is chosen as $T_r(t=0) \sim \mathcal{T}(\mathcal{N}(30, 3), 25, 35)$ where the mean $\mu_{T_r(t=0)} = 30^\circ\text{C}$ and is taken from Table 2 and the standard deviation $\sigma_{T_r(t=0)} = 3$ is the initial deviation that is assumed. Similarly, the prior for $T_r(t=0)$ is truncated between 25°C and 35°C . The priors of $T_s(t=0)$ and $T_{Fe}(t=0)$ are also set accordingly with variance = 3 and the mean value taken from Table 2 within some relevant values of θ_{min} and θ_{max} for the parameters. Priors of other parameters to be found are also set accordingly from Table 2. It is important to note that the posterior distributions are approximated based on the numerical solution of Eq. (9) using different sampling methods. It is out of the scope of this paper to detail sampling methods. Some of the available sampling methods are listed in Table 3 and usage of these sampling algorithms can be found in [19]. We have chosen the NUTS sampler with the number of particles in the sampling as $N_s = 1000$ to estimate the parameters.

C. ESTIMATED PARAMETERS

The posterior distributions of the estimated heat transfer parameters are shown in Fig. 5. Figure 5 (a) shows the distribution of the variance \mathcal{V} of the measurement noises.

TABLE 3. Priors, data and sampling methods.

Prior distributions	Data	Sampling
$\nu \sim \Gamma^{-1}(2, 3)$ $T_r(t=0) \sim \mathcal{T}(\mathcal{N}(30, 3), 25, 35)$, $UA_{r2\delta} \sim \mathcal{T}(\mathcal{N}(2.7, 1), 0.2, 5)$, $\dot{Q}_{Fe}^\sigma \sim \mathcal{T}(\mathcal{N}(212, 40), 20, 400)$, etc.	$y = [y_1 \ y_2 \ \dots \ y_N]$ $u = [u_1 \ u_2 \ \dots \ u_N]$	1. Importance sampling (IS) 2. Sequential Monte Carlo (SMC) 3. Metropolis-Hastings (MH) 4. Hamiltonian Monte Carlo (HMC) 5. No-U-Turn Sampler (NUTS) 6. Particle Gibbs sampling (PG)

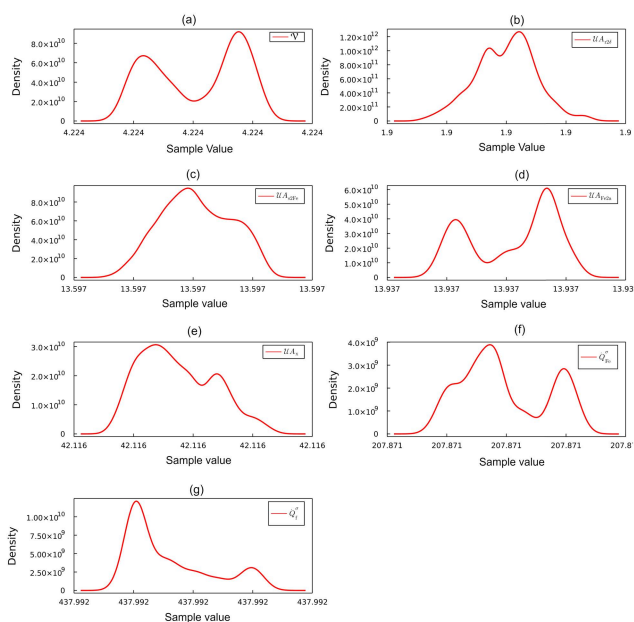


FIGURE 5. Posterior distribution of heat transfer parameters for the thermal model of the air-cooled synchronous generator.

Figures 5 (b-g) show the posterior distributions of heat transfer parameters with mean and variance as shown in Table 4. The expected value of these distributions are used as the estimated parameters. Similarly, Fig. 6 shows the estimated initial conditions for the metal temperatures of the air-cooled generators.

D. ANALYSIS OF ESTIMATED PARAMETERS

The estimated parameters are analyzed based on mean and standard deviation as well as naive standard error (Naive SE) [22], and effective sample size (ESS) [23] as shown in Table 4.

1) NAIVE STANDARD ERROR (NAIVE SE)

Naive SE is a term defined for inferential statistics similarly to the mean and the standard deviation defined for descriptive statistics. Naive SE is computed as in [22]. Naive SE provides a measure of the potential error in the estimate while parameter inference is done through Bayes’ theorem. Naive SE

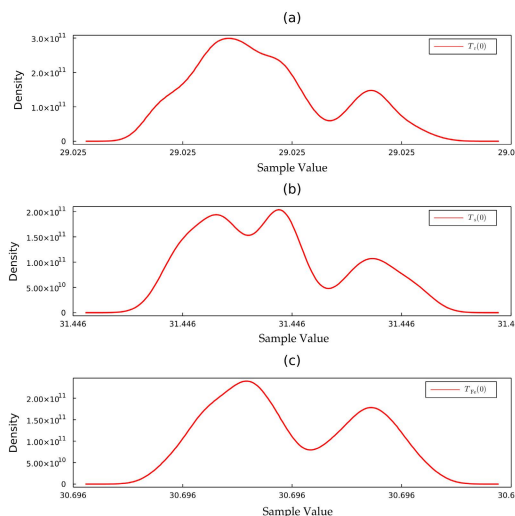


FIGURE 6. Posterior distribution of initial values for the thermal model of the air-cooled synchronous generator.

TABLE 4. Analysis of the Bayesian inference using NUTS sampler for the estimation of initial values, heat transfers and heat sources parameters for air-cooled generator.

Parameter	Mean	Std.	Naive SE $\hat{\sigma}_\theta$	ESS
ν	4.22	$5.87 \cdot 10^{-12}$	$1.85 \cdot 10^{-13}$	2.16
$T_r(t=0)$	29.02	$1.49 \cdot 10^{-12}$	$4.74 \cdot 10^{-14}$	4.92
$T_s(t=0)$	31.44	$2.08 \cdot 10^{-12}$	$6.48 \cdot 10^{-14}$	2.61
$T_{Fe}(t=0)$	30.69	$1.83 \cdot 10^{-12}$	$6.12 \cdot 10^{-14}$	2.36
$UA_{r2\delta}$	1.90	$3.35 \cdot 10^{-13}$	$1.06 \cdot 10^{-14}$	12.70
UA_{s2Fe}	13.59	$3.98 \cdot 10^{-12}$	$1.25 \cdot 10^{-13}$	10.77
UA_{Fe2a}	13.92	$1.01 \cdot 10^{-11}$	$3.20 \cdot 10^{-13}$	2.24
UA_x	42.11	$1.26 \cdot 10^{-11}$	$4.00 \cdot 10^{-13}$	4.35
\dot{Q}_{Fe}^σ	207.87	$1.29 \cdot 10^{-10}$	$4.08 \cdot 10^{-12}$	2.57
\dot{Q}_f^σ	437.99	$6.31 \cdot 10^{-11}$	$1.99 \cdot 10^{-12}$	2.65

calculates the width of sample means around the population mean. The lower the value of naive SE, the lower is the dispersion. Naive SE can also be used to find the upper and lower limit for the 95% confidence interval of the parameter given by $\bar{\theta} \pm \hat{\sigma}_\theta$ where $\bar{\theta}$ is the mean value of the parameter and $\hat{\sigma}_\theta$ is the naive SE.

From Table 4 we see that Naive SE measuring the dispersion of sample means around the population mean, in the case of initial conditions lies between $4.74 \cdot 10^{-14}$ to $6.48 \cdot 10^{-14}$.

The ratios of Naive SE for initial values is $\hat{\sigma}_{T_r} : \hat{\sigma}_{T_s} : \hat{\sigma}_{T_{Fe}} = 4.74 : 6.48 : 6.12$. Since $T_r(t = 0)$ has lower Naive SE, the posterior distributions of $T_s(t = 0)$ and $T_{Fe}(t = 0)$ are wider than the posterior distribution of $T_r(t = 0)$. This shows that the posterior distribution of the temperature of the initial states related to the rotating copper inside the hydro generator is less wider than that of stationary copper and iron.

From Table 4 we see that the naive SE in the case of heat transfer from rotor copper to the air-gap $\mathcal{U}_{A_{r2\delta}}$ is smaller as compared to the heat transfer from the stator copper to stator iron $\mathcal{U}_{A_{s2Fe}}$ and the heat transfer from iron to air $\mathcal{U}_{A_{Fe2a}}$. Thus, the posterior distribution of the heat transfer parameter related to the air is more narrower than the heat transfer parameter related to the metal inside the hydro generator. From the values of the naive SE from Table 4 in the case of heat sources parameters of the hydro generator, the dispersion in the posterior distribution of the iron heat source parameter \dot{Q}_{Fe}^σ is higher than that of the friction heat source parameter \dot{Q}_f^σ indicating that the heat source parameter related to air is less wider than the metals.

2) EFFECTIVE SAMPLE SIZE (ESS)

ESS describes the correlation between observations in the sample [23]. The calculation of ESS in Turing.jl is performed as in [24]. The higher the value of ESS, the higher is the correlation between the observations in the sample. ESS also helps to determine the relative sampling efficiency of the estimates based on the correlation between the observations in the sample. The relative sampling efficiency of the parameters from the estimated ESS can be calculated as

$$\hat{\eta}_\theta = 1 - \frac{ESS_{\theta_j}}{\sum ESS_{\theta_j}} \tag{10}$$

The smaller the value of ESS, the higher is the sampling efficiency. From Table 4, the relative sampling efficiency $\hat{\eta}$ among the initial conditions $T_r(t = 0)$, $T_s(t = 0)$, and $T_{Fe}(t = 0)$, the relative sampling efficiency of stator iron temperature $T_{Fe}(t = 0)$ is higher as compared to the relative sampling efficiency of $T_r(t = 0)$ and $T_s(t = 0)$. In addition comparing all the temperatures, the rotor copper temperature $T_r(t = 0)$ has the lowest sampling efficiency. This shows that the temperature related to the rotating part of the hydro generator has lower sampling efficiency than the stationary part of the hydro generators. The sampling efficiency of the temperatures can be calculated using Eq. (10). The sampling efficiency for rotor copper temperature is given as $\hat{\eta}_{T_r} = 1 - \frac{4.92}{4.92+2.61+2.36} \approx 0.5$. The ratios of sampling efficiency for temperatures is $\hat{\eta}_{T_r} : \hat{\eta}_{T_s} : \hat{\eta}_{T_{Fe}} \approx 0.5 : 0.73 : 0.76$. Similarly from Table 4 using the estimated ESS for the heat transfer parameters, the relative sampling efficiency of heat transfer from rotating rotor copper to air-gap $\mathcal{U}_{A_{r2\delta}}$ is lower as compared to heat transfer between stationary copper to stationary iron $\mathcal{U}_{A_{s2Fe}}$ or heat transfer from stationary iron to air $\mathcal{U}_{A_{Fe2a}}$. Similarly from Table 4, we can see that both heat source parameters have the same sampling efficiency.

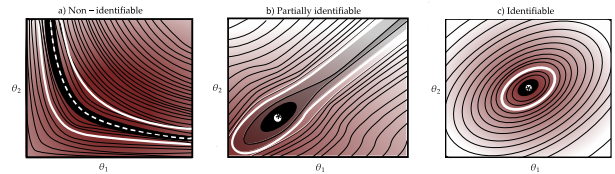


FIGURE 7. Parameters identifiability based on the joint posterior probability distribution of the parameters based on [27].

E. PARAMETER IDENTIFIABILITY

Parameter identifiability tells whether a parameter can be computed uniquely from the given model structure and observations. For complex systems, the number observed quantities is much smaller than the number of states + algebraic variables. It is therefore of interest to estimate the distribution of parameters that can explain the experimental data well. In inferential statistics, the joint posterior distribution of parameters found in Section IV using the Bayesian method can be used for parameter identifiability analysis. In frequentist statistics, profile likelihood projections are used for parameter identifiability [25], [26], [27]. Parameter non-identifiability occurs due to (i) indistinguishability of parameters in the model structure, and (ii) insufficiency in the experimental data. Identifiability analysis considering model structure is termed structural identifiability and identifiability analysis considering the amount and quality of experimental data is termed practical identifiability. Structural identifiability is out of the scope of the paper and our focus is on practical identifiability analysis. Figure 7 shows three cases of the joint posterior probability distribution of parameters θ_1 and θ_2 where Fig. 7 (a) illustrates that both parameters are structurally non-identifiable since the parameters do not converge to a point. The white lines show the posterior high density interval (HDI) within which an unobserved parameter value falls with a particular probability. The white dashed line indicates that the parameters diverge to infinity. The non-identifiability in parameters can only be resolved after the model structure is distinguishable with parameters. In Fig. 7 (b), the parameters are partially identifiable only at the lower density interval. The partially identifiable parameters are denoted as practically non-identifiable parameters. Identifiability of practically non-identifiable parameters can be improved by increasing the amount and the quality of the experimental data. Finally, Fig. 7 (c) shows that parameters converge to a point and are identifiable.

Figure 8 shows the posterior joint probability distribution or the marginal kernel density estimate of heat transfer parameter $\mathcal{U}_{A_{r2\delta}}$ with other heat transfer and heat source parameters. The central region in the marginal posterior distribution shows the HDI for the parameter space with a higher confidence region for the estimated parameters. Since the joint density plot of other heat transfer and heat source parameters bounded within a region, all the heat transfer and heat source parameters are identifiable. The joint points in the central region bounded with distorted ellipses in the figure show the

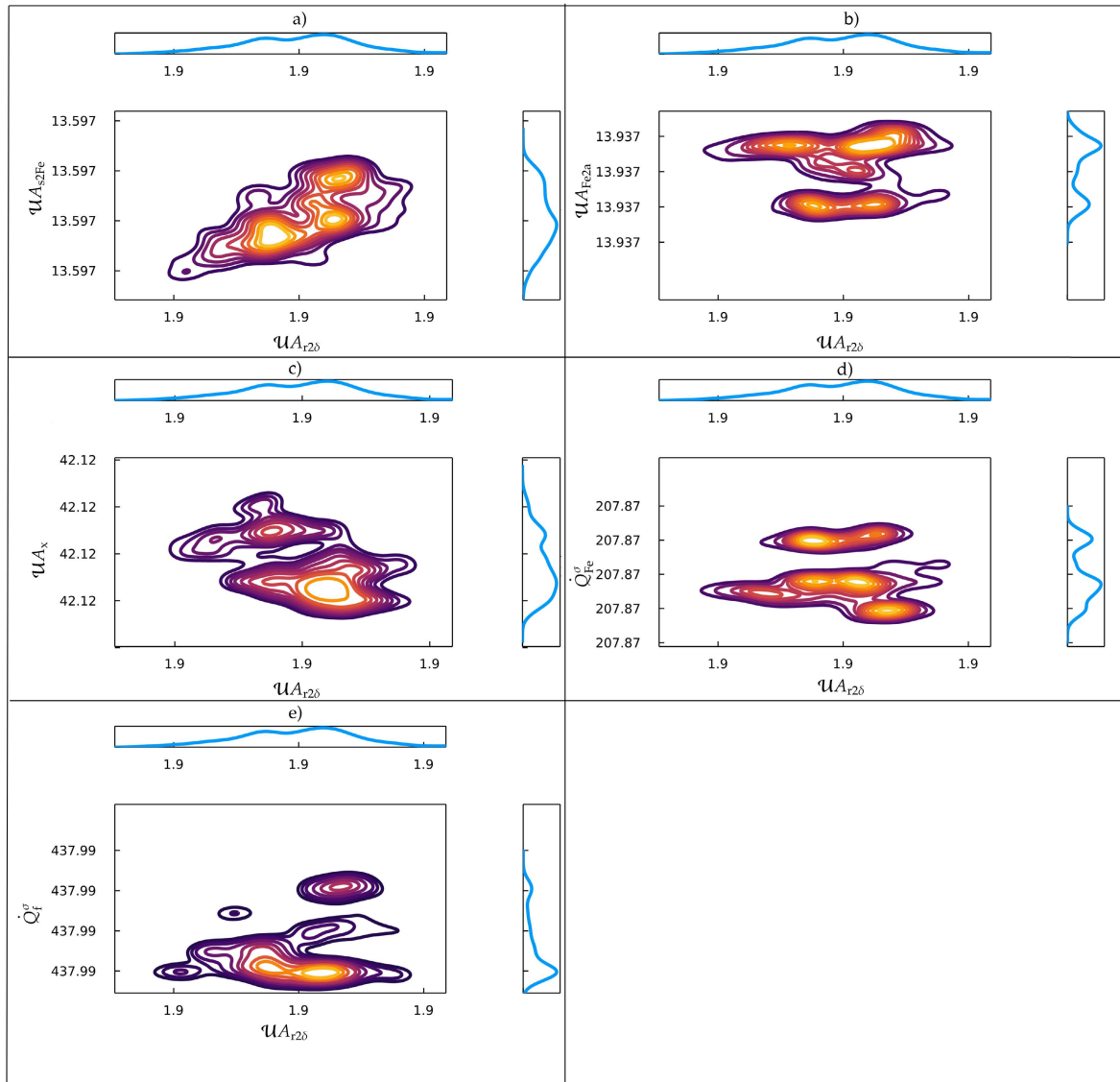


FIGURE 8. Marginal kernel density plot of $UA_{r2\delta}$ with other heat transfer and heat sources parameters.

modal values of the parameters. The joint posterior probability distribution of UA_{s2Fe} with other heat transfer and heat sources parameters, and so on, are not shown in the figure. The identifiability of all the parameters and initial conditions can also be inferred directly from the posterior distribution of the parameters shown in Figs. 5 and 6, respectively.

F. MODEL FITTING

It is of interest to see how well the mathematical model fits with the experimental data. The estimated initial conditions and parameters are used to compare the fitted model with the experimental data.

Figure 9 shows the simulation versus experiment using the estimated parameters for the simulation. The model represents the experimental data well. In the figure, experimental data are well-matched with the simulation in the case of the

stator copper temperature T_s and cold air temperature T_a^c . The experimental data and the simulation are less well matched for the lower temperature region before $t \approx 300$ s in the case of stator iron temperature T_{Fe} and hot air temperature T_a^h .

In the case of T_{Fe} , the mismatch between the experiment and the simulation prior to $t \approx 300$ s as shown in Fig. 9 is caused by the influence of the heat transfer parameter. The posterior distributions of the heat transfer parameter UA_{Fe2a} and UA_{s2Fe} related to stationary parts are more wider than the heat transfer parameter $UA_{r2\delta}$ related to rotating parts. $UA_{r2\delta}$ is the heat transfer related to the rotating copper, UA_{s2Fe} is the heat transfer related to stationary copper, and UA_{Fe2a} is the heat transfer related to stationary iron. From this result, we can infer the dispersion characteristics of the posterior distribution of the stationary copper, stationary iron, and rotating copper in the case of the air-cooled

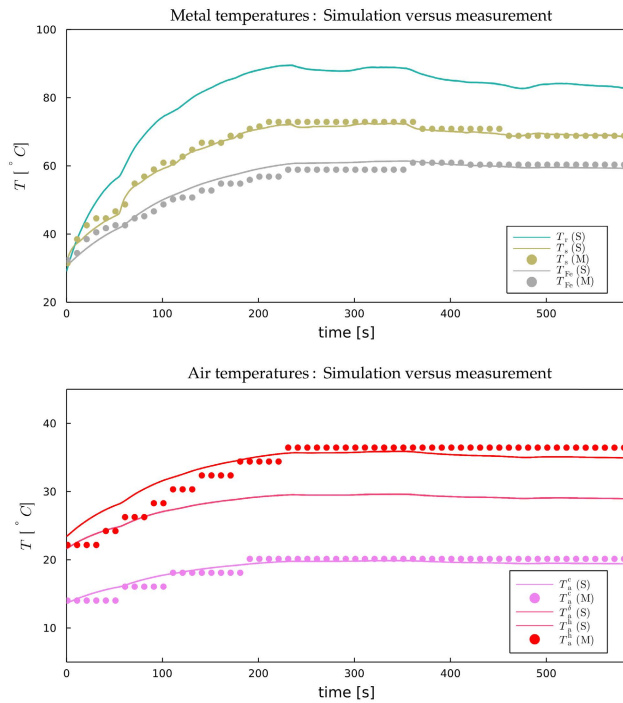


FIGURE 9. Model fit of simulation versus experimental measurements. In the figure, T_r (S), and T_r (M) represent simulated and measured rotor copper temperature, respectively.

synchronous generator. The posterior distribution of the heat transfer parameters related to the stationary parts is more wider than the posterior distribution of the heat transfer parameters related to the rotating parts. The stationary iron receives heat from the heated stator copper at temperature T_s because of terminal current I_t flowing through the stator copper. Thus, the posterior distribution of heat transfer parameter related to stationary iron is more wider. This is because of the result from Section IV-D that the posterior distribution of the heat transfer parameter related to iron receiving heat from the stationary copper \mathcal{UA}_{s2Fe} and the heat transfer from heated stationary iron to air \mathcal{UA}_{s2Fe} are more wider. Thus, the simulation results of the stator iron T_{Fe} is not matched with the experimental data for lower temperature region before $t \approx 300$ s for the air-cooled synchronous generator. In the real operation of the air-cooled hydro generator at Åbjøra, Norway [15], for a period with the average time constant of 53 min the machine was in the state of the cold-run as described in Section II-B. The stationary iron takes time to get heated from the stationary copper heated from the terminal current I_t .

Similarly, in the case of hot air temperature T_a^h , the mismatch between the experiment and the simulation before $t \approx 300$ s as shown in Fig. 9 is because of the influence of the heat transfer parameter related to the stationary iron; \mathcal{UA}_{Fe2a} and \mathcal{UA}_{s2Fe} . From Fig. 1 the iron heat source $\dot{Q}_{Fe2a} = \mathcal{UA}_{Fe2a}(T_{Fe} - T_a^h)$ [16] which indicates that the non-homogeneous heating of iron during the cold-run of the hydro generator cause heat transfer parameter related to stationary

iron \mathcal{UA}_{Fe2a} to attain different modal values as shown in Fig. 5 (c). In addition, this non-homogeneous heating of the iron also affect the iron heat source parameter \dot{Q}_{Fe}^c as shown in Fig. 5 (e). This means that during the cold-run of the air-cooled synchronous generator the air inside the hydro generator at temperature T_a^h is heated intermittently or non-homogeneously as indicated by the experimental data during the cold-run prior to $t \approx 300$ s. Similar, intermittency can be seen in the case of experimental data for cold air temperature T_a^c and stationary iron temperature T_{Fe} . As the air temperatures T_a^c , T_a^δ and T_a^h inside the machine are inter-related through governing Eqs. (3), (4), and (5), it can be predicted that the experimental data during the cold-run of the hydro generator for air-gap temperature T_a^δ should also be intermittent. The governing equations for the metal and air temperatures formulating a dynamic model for the air-cooled machines with stationary iron parts need intermittent correction for its heat transfer parameter related to iron during the cold-run of the machine.

V. CONCLUSION

For the air-cooled synchronous generator as described in Section II-A, results from the analysis of the estimated parameters as described in Section IV-D show that the posterior distribution of temperatures of the stationary parts inside the air-cooled synchronous generator is more wider than the rotating parts. In the case of the heat transfer parameters, the posterior distribution of the heat transfer parameters related to metals is more wider than the posterior distribution of the air-related parameters. Furthermore results also indicate that the posterior distribution of the heat sources parameters related to iron is also more dispersed than other heat sources parameters like heat source due to friction, etc.

From Section IV-E, results indicate that all the parameters estimated are practically identifiable. From Section IV-F, results indicate that the mismatch between the experimental data and the simulation results for the iron temperature and hot air temperature during the cold-run of the hydro generator is due to the higher dispersion characteristics in the posterior distribution of the stationary parts of the generator. The stationary iron takes time to get heated from the stationary copper. The stationary copper gets heated from the terminal current flowing through the stator copper. Thus, the posterior distribution of parameters for the air-cooled synchronous generator affects the mismatch between experimental data and the simulation results. Results also indicate that the heat transfer parameter related to iron attains an intermittent value during the cold-run of the air-cooled synchronous generator.

VI. FUTURE WORK

The governing equations for the air-cooled hydro generator, represented by Eqs. (1-6), are considered with constant metal resistances and constant specific heat capacities. Future work includes parameter estimation and identifiability in the case of temperature dependent resistances and specific heat capacities. From Figs. 5 and 6, we see extremely narrower

parameter distribution. It would be interesting to see the relationship between the measurement data available for the descriptor and the width of parameter distribution.

REFERENCES

- [1] M. Pandey and B. Lie, "The role of hydropower simulation in smart energy systems," in *Proc. IEEE 7th Int. Conf. Energy Smart Syst. (ESS)*, May 2020, pp. 392–397.
- [2] M. Pandey, D. Winkler, R. Sharma, and B. Lie, "Using MPC to balance intermittent wind and solar power with hydro power in microgrids," *Energies*, vol. 14, no. 4, p. 874, Feb. 2021.
- [3] I. Graabak and M. Korpás, "Balancing of variable wind and solar production in continental Europe with Nordic hydropower—A review of simulation studies," *Energy Proc.*, vol. 87, pp. 91–99, Jan. 2016.
- [4] I. Graabak, S. Jaehnert, M. Korpás, and B. Mo, "Norway as a battery for the future European power system—Impacts on the hydropower system," *Energies*, vol. 10, no. 12, p. 2054, Dec. 2017.
- [5] I. Graabak, M. Korpás, S. Jaehnert, and M. Belsnes, "Balancing future variable wind and solar power production in Central-West Europe with Norwegian hydropower," *Energy*, vol. 168, pp. 870–882, Feb. 2019.
- [6] T. Øyvang, J. K. Noland, R. Sharma, G. J. Heggli, and B. Lie, "Enhanced power capability of generator units for increased operational security using NMPC," *IEEE Trans. Power Syst.*, vol. 35, no. 2, pp. 1562–1571, Mar. 2019.
- [7] P. Khadka, D. Winkler, and T. Øyvang, "Online monitoring of a synchronous generator's capability with MATLAB," in *Proc. Linköping Electron. Conf., Västerås, Sweden*, Jan. 2020, pp. 198–205.
- [8] A. Boglietti, A. Cavagnino, D. Staton, M. Shanel, M. Mueller, and C. Mejuto, "Evolution and modern approaches for thermal analysis of electrical machines," *IEEE Trans. Ind. Electron.*, vol. 56, no. 3, pp. 871–882, Mar. 2009.
- [9] A. M. El-Refai, N. C. Harris, T. M. Jahns, and K. M. Rahman, "Thermal analysis of multibarrier interior PM synchronous machine using lumped parameter model," *IEEE Trans. Energy Convers.*, vol. 19, no. 2, pp. 303–309, Jun. 2004.
- [10] S. Nategh, O. Wallmark, M. Leksell, and S. Zhao, "Thermal analysis of a PMaSRM using partial FEA and lumped parameter modeling," *IEEE Trans. Energy Convers.*, vol. 27, no. 2, pp. 477–488, Jun. 2012.
- [11] N. Rostami, M. R. Feyzi, J. Pyrhönen, A. Parviainen, and M. Niemelä, "Lumped-parameter thermal model for axial flux permanent magnet machines," *IEEE Trans. Magn.*, vol. 49, no. 3, pp. 1178–1184, Mar. 2013.
- [12] F. Marignetti, V. D. Colli, and Y. Coia, "Design of axial flux PM synchronous machines through 3-D coupled electromagnetic thermal and fluid-dynamical finite-element analysis," *IEEE Trans. Ind. Electron.*, vol. 55, no. 10, pp. 3591–3601, Oct. 2008.
- [13] Y.-K. R. Chin, E. Nordlund, and A. Staton, "Thermal analysis-lumped-circuit model and finite element analysis," in *Proc. 6th Int. Power Eng. Conf.*, 2003, pp. 952–957.
- [14] B. Zhang, R. Qu, W. Xu, J. Wang, and Y. Chen, "Thermal model of totally enclosed water-cooled permanent magnet synchronous machines for electric vehicle applications," in *Proc. Int. Conf. Electr. Mach. (ICEM)*, Sep. 2014, pp. 2205–2211.
- [15] T. Øyvang, J. K. Noland, G. J. Heggli, and B. Lie, "Online model-based thermal prediction for flexible control of an air-cooled hydrogenerator," *IEEE Trans. Ind. Electron.*, vol. 66, no. 8, pp. 6311–6320, Aug. 2018.
- [16] M. Pandey, "Model fitting and state estimation for thermal model of synchronous generator," M.S. thesis, Dept. Technol., Natural Sci. Marine Sci., Univ. South-Eastern Norway, Notodden, Norway, 2019.
- [17] K. Aleikish, "Hybrid machine learning and mechanistic thermal model of synchronous generator," M.S. thesis, Dept. Sci. Elect. Power Eng., Univ. South-Eastern Norway, Notodden, Norway, 2020.
- [18] T. Øyvang, "Enhanced power capability of generator units for increased operational security," Ph.D. dissertation, Univ. South-Eastern Norway, 2018.
- [19] H. Ge, K. Xu, and Z. Ghahramani, "Turing: A language for flexible probabilistic inference," in *Proc. Int. Conf. Artif. Intell. Statist. (AISTATS)*, Playa Blanca, Spain, Apr. 2018, pp. 1682–1690. [Online]. Available: <http://proceedings.mlr.press/v84/ge18b.html>
- [20] C. Rackauckas and Q. Nie, "DifferentialEquations.jl—A performant and feature-rich ecosystem for solving differential equations in Julia," *J. Open Res. Softw.*, vol. 5, no. 1, p. 15, May 2017.
- [21] Wikipedia. (2020). *Inverse-Gamma Distribution*. Accessed: Oct. 10, 2021. [Online]. Available: https://en.wikipedia.org/wiki/Inverse-gamma_distribution/
- [22] Stack Exchange. (2020). *Naive SE vs Time Series SE: Which Statistics Should I Report After Bayesian Estimation?* Accessed: Oct. 10, 2021. [Online]. Available: <https://stats.stackexchange.com/questions/74450/naive-se-vs-time-series-se-which-statistics-should-i-report-after-bayesian-esti>
- [23] Wikipedia. (2020). *Effective Sample Size*. Accessed: Oct. 10, 2021. [Online]. Available: https://en.wikipedia.org/wiki/Effective_sample_size
- [24] K. Xu, "Probabilistic programming in Julia new inference algorithms," M.S. thesis, Univ. Cambridge, Cambridge, U.K., 2016.
- [25] N. R. Kristensen, H. Madsen, and S. B. Jørgensen, "Parameter estimation in stochastic grey-box models," *Automatica*, vol. 40, no. 2, pp. 225–237, Feb. 2004.
- [26] O. M. Brastein, A. Ghaderi, C. F. Pfeiffer, and N.-O. Skeie, "Analysing uncertainty in parameter estimation and prediction for grey-box building thermal behaviour models," *Energy Buildings*, vol. 224, Oct. 2020, Art. no. 110236.
- [27] A. Raue, C. Kreutz, T. Maiwald, J. Bachmann, M. Schilling, U. Klingmüller, and J. Timmer, "Structural and practical identifiability analysis of partially observed dynamical models by exploiting the profile likelihood," *Bioinformatics*, vol. 25, no. 15, pp. 1923–1929, 2009.



MADHUSUDHAN PANDEY received the M.Sc. degree in electrical power engineering from the University of South-Eastern Norway (USN), Norway, in 2019. Since 2019, he has been a Ph.D. Researcher with TMCC, USN, Porsgrunn, Norway. His research interests include modeling, control, and optimization of dynamic systems and integration of dispatchable renewable energy sources with variable renewable energy sources.



BERNT LIE (Member, IEEE) received the Ph.D. degree in engineering cybernetics from the Norwegian University of Science and Technology (NTNU), Norway, in 1990. From 1987 to 1991, he was an Assistant and an Associate Professor at NTNU. In 1992, he joined at the University of South-Eastern Norway, where he is currently a Professor in informatics and the Leader of the Telemark Modeling and Control Center. His research interests include control relevant modeling and advanced control, with applications mainly within the process and energy industries.

...